# Isotope effect on the soft-mode dynamics of SrTiO₃ studied by Raman scattering

H. Taniguchi* and T. Yagi

*Research Institute for Electronic Science, Hokkaido University, Sapporo 060-0812, Japan*

M. Takesada

*Department of Physics, Hokkaido University, Sapporo 060-0810, Japan*

M. Itoh

*Materials and Structure Laboratory, Tokyo Institute of Technology, Yokohama 226-8503, Japan*

The oxygen isotope effect on the soft-mode dynamics in quantum paraelectric $SrTi(^{18}O_x{}^{16}O_{1-x})_3$ [STO18-$x$] is investigated by Raman scattering in terms of local symmetry breaking in the paraelectric phase. The exchange rates $x$ of the $^{18}O$ atoms are 0.23 [STO18-23] and 0.32 [STO18-32], which are less than the critical value $x_c(=0.33)$. In STO18-32, whose exchange rate is just below $x_c$, the soft $E_u$ mode shows hardening behavior in a low-temperature region indicating the onset of local ferroelectric order. On the other hand, the soft $E_u$ mode in STO18-23 does not show any hardening behavior until 0 K. The enhancement of the inhomogeneity in the crystal by the exchange of $^{18}O$ is concluded to play an essential role in the soft-mode dynamics of the quantum paraelectric and ferroelectric STO18-$x$. The relation between the soft-mode dynamics and quantum fluctuation is discussed.

DOI: 10.1103/PhysRevB.72.064111        PACS number(s): 77.84.Dy, 77.80.Bh, 78.30.$-$j

## I. INTRODUCTION

Strontium titanate SrTiO₃ (STO16) shows the quantum paraelectricity in a low-temperature region, that is, the dielectric constant of STO16 increases rapidly with decreasing temperature but saturates at a huge value, $\epsilon' \approx 2 \times 10^4$, near 0 K due to the quantum fluctuation. In association with the dielectric behavior, the transverse optic soft mode also does not freeze until 0 K due to the quantum fluctuation, as indicated by the Lyddane-Sachs-Teller relation.[1–3] The ferroelectric order of STO16 can be induced by application of a small external field such as electric bias[4] or uniaxial stress[5] to suppress the quantum fluctuation. Recently, Itoh *et al.* discovered that the ferroelectricity is also induced by the exchange of $^{16}O$ for its isotope $^{18}O$ with the exchange rate more than 33%.[6–8] The ferroelectricity has been confirmed by the observation of the *D-E* hysteresis loop below $T_c$ accompanied with the sharp peak of the dielectric constant.[6–9] This phenomenon has attracted much attention since its discovery because of a successful example of the artificial control of the quantum fluctuation by the isotope exchange.

In order to elucidate the phase-transition mechanism of ferroelectric $SrTi(^{18}O_x{}^{16}O_{1-x})_3$ [STO18-$x$], many studies have been reported in the experimental and the theoretical approach.[10–14] A series of light-scattering experiments on nearly fully exchanged STO18-$x$ has observed the ferroelectric soft $E_u$ mode, which softens toward zero-frequency at $T_c$ with less damping than in the other perovskite crystals.[15–17] In particular, the ideal displacive-type ferroelectric phase transition has been recently reported in Ref. 17 for STO18-95. However, it still remains an open question how quantum paraelectric SrTiO₃ changes into the ferroelectric one by the increase of exchange rate of the oxygen isotope $^{18}O$. In order to clarify the mechanism of the isotopic induction of ferroelectricity, the change of the soft-mode dynamics with in-

creasing the exchange rate is needed to be investigated in quantum paraelectric STO18-$x$, whose exchange rate is less than $x_c$.

For the investigation of the soft-mode dynamics, the Raman scattering experiment is quite a suitable method because of its frequency resolution and sensitivity. In the Raman scattering experiment on STO18-$x$, however, the observation of the soft mode is generally limited to the ferroelectric phase of STO18-$x$ ($x > x_c$) because of the macroscopic centrosymmetry of the crystal. In our previous paper, the observation of the Raman spectrum of the soft $E_u$ mode has been reported in the paraelectric phase of STO18-$x$ whose exchange rate is less than $x_c$.[18,19] The soft $E_u$ mode, though it is nominally Raman-inactive, is activated optically by the local symmetry breaking. This result indicates that the Raman scattering experiment is possible to investigate the dynamics of the soft mode even in quantum paraelectric STO18-$x$ ($x < x_c$). In the present study, the isotope effects on the soft-mode dynamics and the local symmetry breaking are investigated systematically in the nonexchanged STO16, STO18-23, and STO18-32 whose exchange rate is critically close to $x_c$ but less than it. Finally, the soft-mode dynamics in the quantum paraelectric STO18-$x$ ($x < x_c$) is discussed in connection with the isotope effect on the quantum fluctuation.

## II. EXPERIMENTAL METHOD

Single-crystal plates of STO16 were cut with the $(110)_c$ surfaces and the dimensions $7.0 \| [001]_c \times 3.0 \| [\bar{1}10]_c \times 0.5 \| [110]_c$ mm³ from a Verneuli-grown single-crystal lump of excellent quality manufactured by Furuuchi Chemical Co. ($[001]_c$ indicates the [001] axis in the cubic system). These dimensions were chosen in order to obtain a tetragonal
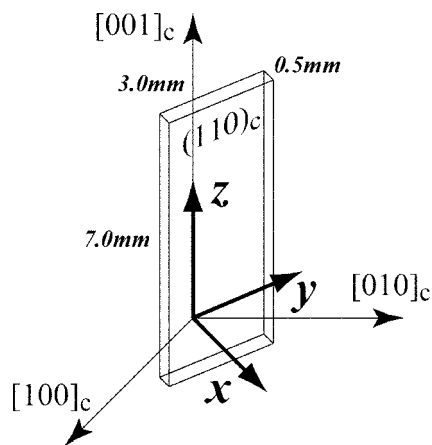
FIG. 1. Sample dimensions and tetragonal axial setting ($x$, $y$, and $z$ axes). See text for the details.

monodomain with the $c$ axis parallel to the $[001]_c$ direction below the cubic-to-tetragonal phase-transition temperature. The surfaces of all specimens were polished to optical quality. Oxygen-isotope exchange was performed by heating the plates at 1323 K in $^{18}O_2$ atmosphere. The final exchange rate $x$ of specimen was determined from the increment of the weight.

Raman scattering experiments were performed on STO18-23, STO18-32, and nonexchanged STO16. The exchange rates were chosen in order to investigate systematically the induction process of ferroelectricity. The crystallographic axes are denoted by a tetragonal set as follows: $x \| [110]_c$, $y \| [\bar{1}10]_c$, and $z \| [001]_c$ (Fig. 1). An Ar$^+$-ion laser at a wavelength of 514.5 nm was used for the light source with an output power of 100 mW. The vertically polarized incident beam penetrates the sample along the $x$ axis. The Raman scattering spectra were observed in the backscattering geometries $x(yy)\text{-}x$ and $x(yz)\text{-}x$ with the scattering vector $Q \| [110]_c$. The light scattered from the specimen was dispersed using a Jovin-Yvon T64000 triple monochromator with the subtractive dispersion mode and detected with a liquid nitrogen-cooled CCD camera. The spectral resolution of the present system attains 1.5 cm$^{-1}$ half-width at half maximum.

In order to observe the Raman spectra until below 1 K, we prepared the specially designed $^3$He optical cryostat TS-HE3-C9 (Taiyo Toyo Sanso Co.). This cryostat employs both $^4$He pumping type cooling and $^3$He evaporation type cooling using a charcoal adsorbent. The collaborative use of these two methods attained 520 mK on the specimens under a 100 mW laser irradiation input. The temperature of the specimen was controlled by a TS-3H100-C temperature controller within ±0.05 K.

## III. RESULTS

The $x(yy)\text{-}x$ Raman scattering spectra of STO16 in the frequency range from 9 to 80 cm$^{-1}$ are observed in the backscattering geometry as a function of temperature [Fig. 2(a)]. A broad component indicated by the broken line in the figure
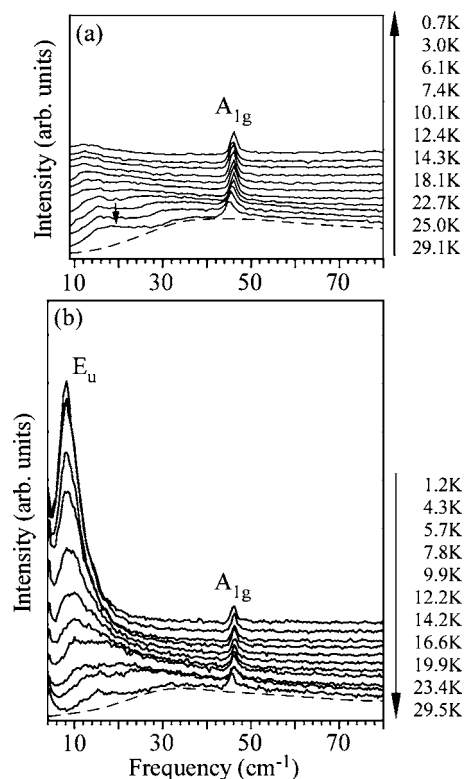


FIG. 2. Raman scattering spectra of (a) STO16 and (b) STO18-23 observed in the $x(yy)\text{-}x$ geometry at several temperatures. Each $A_{1g}$ mode at 45 cm$^{-1}$ is indicated by an arrow. Broken lines are guides to the eye for the broad components.

and the small shoulder pointed out by an arrow are observed at a high-temperature region. These two components shift to the low-frequency region with decreasing temperature. In addition to these components, a sharp peak exists at 45 cm$^{-1}$ and it is assigned to the $A_{1g}$ mode according to previous reports.[4,20] The present result on STO16 is in good agreement with the previous results by Sekine *et al.*[21] and Uwe *et al.*[22] Figure 2(b) shows the $x(yy)\text{-}x$ Raman scattering spectra of STO18-23. In this case, we observed successfully the spectrum in the frequency range from 4 to 80 cm$^{-1}$ in the backscattering geometry. An obvious isotope effect on the spectrum has been observed in the low-temperature region; the small shoulder develops drastically into a sharp peak with decreasing temperature, in contrast to the result of STO16 shown in Fig. 2(a). This phenomenon shows apparently the isotope-exchange effect on the spectrum. The sharp peak has clearly the typical spectral shape of the underdamped phonon well known as the Lorentz-type function. In the low-temperature region, the sharp peak becomes intense but its frequency remains at constant value 8 cm$^{-1}$ until 1.2 K. By a comparison with the hyper-Raman scattering study,[23] the peak frequency 8 cm$^{-1}$ is lower than that of the soft $E_u$ mode of STO16. Therefore, it is reasonable to assign this peak to the spectrum of the soft $E_u$ mode.

The soft $E_u$ mode is nominally Raman-inactive due to the macroscopic centrosymmetry of the paraelectric phase of STO18-23 whose exchange rate is less than the critical exchange rate $x_c$. However, the intense and sharp peak observed in STO18-23 in the low-temperature region below 10
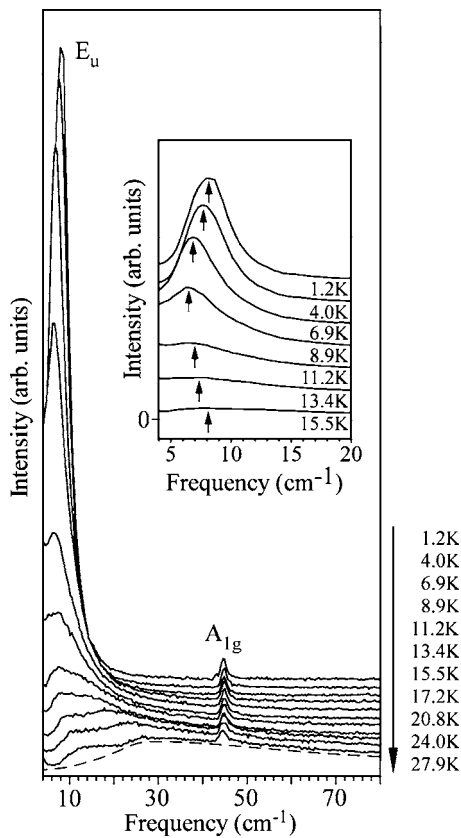
FIG. 3. Raman scattering spectra of STO18-32 observed in the $x(yy)$-$x$ geometry at several temperatures. The $A_{1g}$ mode at 45 cm$^{-1}$ is indicated by an arrow. The broken line is a guide to the eye for the broad component. The inset shows an expanded view of the temperature dependence of the soft $E_u$ mode spectrum in the low-temperature region below 15.5 K. Arrows in the inset indicate the peak positions of the soft $E_u$ mode spectra.



FIG. 4. Raman scattering spectra of (a) STO18-23 and (b) STO18-32 observed in the $x(yz)$-$x$ geometry at several temperatures. See text for details.

K indicates that the Raman-inactive $E_u$ mode would be activated by a symmetry breaking taking place locally in the crystal. We can conclude that the isotope exchange enhances the local symmetry breaking in the low-temperature region. Thus, the local symmetry breaking region (LSBR) developed in the isotope-exchanged crystal.

Figure 3 shows the $x(yy)$-$x$ spectra observed in STO18-32, whose exchange rate is just below $x_c$. This means the exchange rate of $^{18}$O in STO18-32 is critically close to the value where the ferroelectric phase takes place. As shown in Fig. 3, the spectrum of the soft $E_u$ mode is amazingly enhanced with decreasing temperature keeping its narrow spectral width. Finally, the intensity of the sharp peak of STO18-32 becomes almost three times larger than that of STO18-23 at 1.2 K. In the high-temperature region, on the other hand, the broad spectral shape is similar to those of STO16 and STO18-23 as shown in Figs. 2(a) and 2(b). This phenomenon indicates that the development of LSBR is enhanced by the exchange of $^{18}$O especially in the low-temperature region, because the intensity of the Raman spectrum is proportional to the volume of LSBR in the irradiated volume by the laser.

Furthermore, the spectra of STO18-32 show a remarkable behavior of the soft $E_u$ mode in the low-temperature region
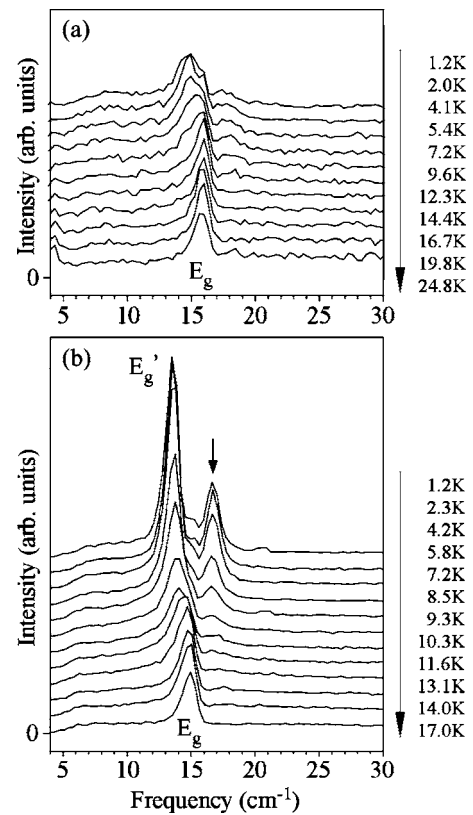
below 10 K as shown in the inset of Fig. 3. As shown in the figure, the soft $E_u$ mode pointed out by arrows decreases its frequency until 9 K. Subsequently, it begins shifting to the high-frequency side. Finally, the soft $E_u$ mode frequency becomes 8 cm$^{-1}$ at 1.2 K. It is a quite new effect and an important phenomenon that the hardening of the ferroelectric soft mode is observed in the paraelectric phase. The paraelectricity is confirmed by the exchange rate of STO18-32 less than $x_c$. The physical origin of this behavior will be discussed later.

The Raman scattering spectra of STO18-23 and STO18-32 observed in the $x(yz)$-$x$ geometry are shown in Figs. 4(a) and 4(b). In the spectra of STO18-23 shown in Fig. 4(a), the $E_g$ mode at 15 cm$^{-1}$ does not show any change except for the broadening seen below 6 K. In contrast to this, the spectrum of STO18-32 shown in Fig. 4(b) exhibits the noticeable change in the low-temperature region. As shown in the figure, the sharp peak indicated by an arrow newly appears at 10 K and increases its intensity with decreasing temperature. On the other hand, the $E_g$ mode spectrum shifts to the low-frequency side by 2 cm$^{-1}$ below 10 K and it becomes more intense with decreasing temperature similarly to the new peak. Finally, a pair of sharp peaks is clearly established at 1.2 K, as shown in Fig. 4(b). The appearance of the new peak is considered to be strong evidence for the occurrence of further symmetry lowering of LSBR in the low-temperature region of STO18-32, and it seems to co-occur with the onset of the hardening of the soft $E_u$ mode shown in

Fig. 3. This result implies the close relation between the further symmetry lowering of LSBR and the soft-mode dynamics. The local symmetry breaking in the crystal is discussed in connection with the soft-mode dynamics in the following section.

## IV. DISCUSSION

### A. Spectrum analysis

In the present study, the nominally Raman-inactive soft $E_u$ modes, which are activated in LSBR, have been observed as the sharp and intense peaks in the low-temperature region of STO18-23 and STO18-32. By analyzing the sharp spectrum, we investigate the soft $E_u$ mode dynamics and the effect of the isotope-exchange on the dynamics. The sharp peak of the soft $E_u$ mode is grown up from the small shoulder, which is also observed in STO16 in the high-temperature region. In the previous results of STO16, the small shoulder was assigned to be caused by the phonon-blanch scattering of the soft $E_u$ mode. In the present study, however, the sharp peaks obviously show the spectral shapes of the underdamped phonon in the low-temperature region, as indicated by the results of STO18-23 and STO18-32. Therefore, we assigned them to single-phonon scattering spectra and analyzed them with a Lorentz-type function.

On the other hand, we estimated the size of LSBR by analyzing the spectral shape of the broad component. The origin of the broad component has been considered to be caused by the phonon-branch scattering of the higher-harmonic component of the soft $E_u$ mode.[22,24,25] In the same way as was done in previous studies, we calculated the spectral shape of the broad component by the phonon-branch scattering model reported by Uwe *et al.*[24] According to this model, the spectral shape of the broad component is given by

$$I(\omega) \propto \int W(q)I'(q,\omega)\mathrm{d}q \qquad (1)$$

with

$$W(q) \propto \frac{1}{1+q^2R^2}, \qquad (2)$$

$$I'(q,\omega) \propto \frac{\omega_q^2\gamma\omega}{(\omega_q^2-\omega^2)^2+\gamma^2\omega^2}, \qquad (3)$$

where $R$ is a size of LSBR normalized by the lattice constant $a(=0.39\ \mathrm{nm})$, and $\gamma$ is a damping constant. $\omega_q=(\omega_0^2+D^2q^2)^{1/2}$ is the soft $E_u$ mode frequency at wave number $q$. For simplification, the phonon dispersion given by $D$ is assumed to be isotropic with the value of 100 meV. In the previous papers, for simplicity, Eq. (1) was calculated with the approximation that the damping of the soft mode is ignored.[22,24,25] That is, the spectral shape of the soft $E_u$ mode was assumed to be a $\delta$ function. However, this approximation does not give any good fit to the frequency part of the broad component lower than $\omega_0$. In the present study, we took the soft-mode damping $\gamma$ into account as independent of wave number. Thus, in order to analyze the spectrum, we
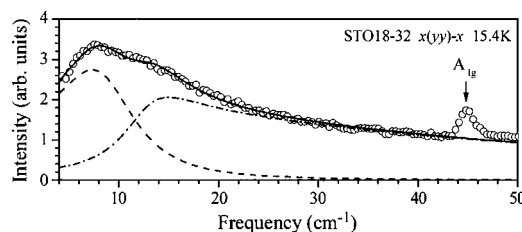


FIG. 5. Two components in the raw spectrum of STO18-32 (open circles) observed in the $x(yy)$-$x$ geometries at 15.4 K. A broken line and a dash-dotted line denote a Lorentzian peak for the $E_u$ mode and the broad component, respectively. The curve indicated by a solid line is obtained by the least-squares method.

stand on the basis that the spectrum is composed of (i) Lorentz-type function of the soft $E_u$ mode spectrum and (ii) the broad component given by the phonon-blanch scattering model. An example of the fit is shown in Fig. 5. The calculated $E_u$ mode spectrum and the broad component are presented by a broken and a dash-dotted line, respectively. As shown in the figure, the superposition of these two components denoted by a solid line well reproduces the spectrum. Finally, the procedure gives satisfactory results for all spectra observed in the present study.

### B. Isotope effect on the growth of LSBR

In Fig. 6, the normalized size of LSBR for each specimen is presented as a function of temperature. The results for STO16, STO18-23, and STO18-32 are denoted by crosses, closed circles, and open squares, respectively. In the low-temperature region below 15 K, a drastic isotope effect on the growth of LSBR is seen in the figure. First, we discuss the isotope effect on the size of LSBR in STO18-23. As shown in Fig. 6, the growth of LSBR in STO18-23 is markedly enhanced by the isotope exchange in the low-temperature region, and finally, it becomes four times larger than that in STO16. In the low-temperature region near 0 K,
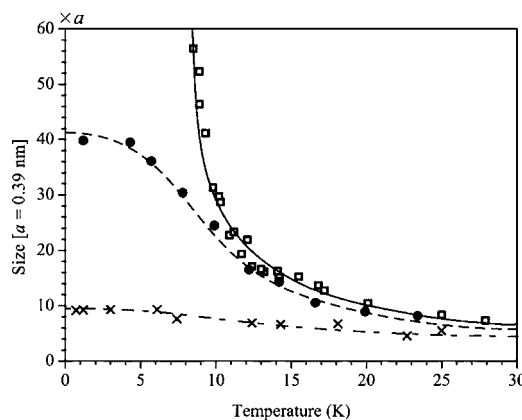


FIG. 6. Temperature dependences of a normalized size of LSBR calculated from the spectra of the broad components of STO16 (crosses), STO18-23 (closed circles), and STO18-32 (open squares) in the scattering geometry $x(yy)$-$x$. A dash-dot line, a broken line, and a solid line are guides to the eye for the results of STO16, STO18-23, and STO18-32, respectively.

the enlarged LSBR in STO18-23 shows the saturated behavior similar to that in STO16. In spite of the marked change in the low-temperature region, little enlargement of LSBR has been found in the high-temperature region of STO18-23 as shown in Fig. 6. It indicates that the isotope exchange enhances the growth of LSBR especially in the low-temperature region. These results suggest that the growth of LSBR is suppressed by quantum fluctuation in STO16. The drastic enhancement of the growth of LSBR in STO18-23 is considered to be caused by the depression of quantum fluctuation by the exchange of $^{16}O$ for $^{18}O$. Since the effect of quantum fluctuation is expected to become more dominant with lowering temperature due to a decrease of thermal fluctuation, the enhancement of the growth of LSBR becomes more marked with decreasing temperature. The saturated behavior of LSBRs in STO16 and STO18-23 is considered to be caused by the temperature independence of quantum fluctuation.

The size of LSBR of STO18-32 shows furthermore the drastic change on the growth with lowering temperature, as shown in Fig. 6. LSBR in STO18-32 begins to develop rapidly; below 9 K, it exhibits a divergent growth. In the low-temperature region below 8 K, the size of LSBR is not presented because the broad component becomes too poor to analyze precisely. The divergent behavior in the low-temperature region of STO18-32 is clearly different from the saturated behavior seen in the low-temperature region of STO16 and STO18-23. It implies the occurrence of the additional mechanism on the growth of LSBR in the low-temperature region of STO18-32. In contrast, the temperature dependence of the size of LSBR in the high-temperature region of STO18-32 is quite similar to that in STO18-23. The onset of the rapid growth of LSBR in STO18-32 is in good accordance with that of the hardening of the soft $E_u$ mode (Fig. 3) and the appearance of a new peak [Fig. 4(b)]. Therefore, the divergent growth of LSBR is considered to be closely related to the soft-mode dynamics and the further symmetry breaking of LSBR suggested by the new peak.

### C. Dynamics of the soft $E_u$ mode and the symmetry of LSBR

The temperature dependences of the soft $E_u$ mode frequencies of STO16, STO18-23, and STO18-32 are presented by closed circles, closed squares, and closed triangles in Figs. 7(a), 7(b), and 7(c), respectively. The half-width at half maximum of the soft $E_u$ mode in each specimen is also presented by corresponding open symbols in the figures. The present result for the $E_u$ mode frequency of STO16 is considerably in good agreement with the result of the previous hyper-Raman experiment [crosses in Fig. 7(a)] in spite of the experimental errors due to the poor intensity of the soft $E_u$ mode.[23] It confirms the reliability of the result of the present analysis. The results for STO18-23 and STO18-32 have smaller errors than that of STO16 because of their excellent signal-to-noise ratio, and clearly show the isotope-exchange effect on the soft $E_u$ mode dynamics, as shown in Figs. 7(b) and 7(c). The frequency of the soft $E_u$ mode is decreased with increasing the exchange rate $x$, and in STO18-32 whose
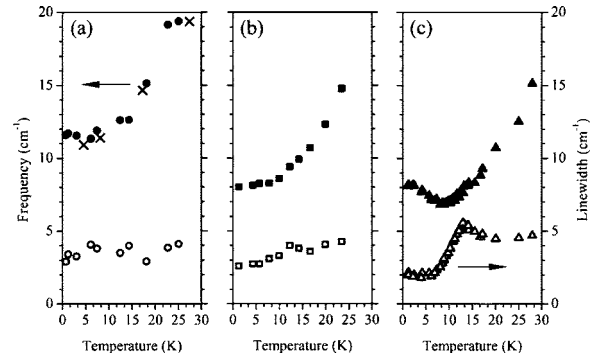


FIG. 7. Temperature dependences of the soft $E_u$ mode in STO16 (closed circles), STO18-23 (closed squares), and STO18-32 (closed triangles) observed in the scattering geometry $x(yy)\text{-}x$. Crosses indicate the previous result for STO16 obtained by the hyper-Raman scattering experiment (Ref. 23). The corresponding open symbol denotes the half-widths at half maximum of the soft $E_u$ mode spectrum of each specimen.

exchange rate is just below $x_c$, it starts to show the hardening behavior in spite of the exchange rate less than $x_c$. In accordance with the hardening behavior, the linewidth of the soft $E_u$ mode exhibits the peaklike anomaly before the frequency minimum, as shown in Fig. 7(c). In this section, we discuss first the isotope effect on the soft $E_u$ mode dynamics in STO18-23 and deduce the symmetry of LSBR from the behavior of the soft $E_u$ mode. Secondly, the hardening behavior of the soft $E_u$ mode is discussed in connection with the simultaneous anomalies observed in the low-temperature region of STO18-32, namely the appearance of the new peak in the $x(yz)\text{-}x$ scattering geometry (Fig. 4) and the divergent growth of LSBR (Fig. 6).

As shown in Fig. 7(b), the frequency of the soft $E_u$ mode decreases with lowering temperature, and finally, it becomes independent of temperature at the frequency of 8 cm$^{-1}$. Compared to the result of STO16 shown in Fig. 7(a), the soft $E_u$ mode frequency of STO18-23 is lowered by 3 cm$^{-1}$ in the entire temperature range observed here. It is considered to be caused by a mass effect on the Slater-type polar mode by the isotope exchange. The soft $E_u$ mode in STO18-23 becomes independent of temperature in the low-temperature region near 0 K. This result clearly indicates that quantum fluctuation, though it is depressed by the isotope exchange, still suppresses the ferroelectric order in the low-temperature region of STO18-23.

Since the Raman-inactive soft $E_u$ mode is activated in LSBR, the behavior of the soft $E_u$ mode also gives information for the symmetry of LSBR; generally, the polar mode is optically activated in the noncentrosymmetric region. The Raman scattering spectra of the polar $E_u$ mode in STO18-23 indicate that the symmetry of the crystal is locally lowered to the noncentrosymmetric one. One can expect that the noncentrosymmetric symmetry in LSBR is the ferroelectric one, which is the same as that in the ferroelectric phase of STO18-$x$ ($x > x_c$) or in the ferroelectric microregion (FMR) reported by Uwe *et al.* If the symmetry of LSBR is ferroelectric, the soft $E_u$ mode must undergo its freezing because the origin of polarization in SrTiO$_3$ is the Slater-type polar

$E_u$ mode. However, the soft $E_u$ mode in STO18-23 does not freeze obviously until 1.2 K, as shown in the figure. Therefore, the symmetry of LSBR developed in the low-temperature region of STO18-23 is concluded to be noncentrosymmetric but is not ferroelectric. It is concluded that the isotope exchange induces the development of LSBR by the depression of quantum fluctuation, but the symmetry of LSBR still remains nonferroelectric in STO18-23.

In Fig. 7(c), the hardening behavior of the soft $E_u$ mode in STO18-32 is clarified by the spectrum analysis in agreement with the result shown in Fig. 3. The frequency of the soft $E_u$ mode in STO18-32 decreases with lowering temperature and takes its minimum at 7 cm$^{-1}$. Then, it begins hardening and finally attains 8 cm$^{-1}$ at 1.2 K. The hardening of the soft $E_u$ mode seems to be accompanied by the appearance of the new peak in the $x(yz)$-$x$ scattering geometry shown in Fig. 4(b). The new peak suggests a further symmetry lowering of LSBR from the nonferroelectric one. Since the exchange rate of STO18-32 is just below $x_c$, the most plausible interpretation for the further symmetry lowering of LSBR is the precursory occurrence of a local ferroelectric region in LSBR before the onset of the ferroelectric state. According to the soft-mode theory, the soft $E_u$ mode is reasonably expected to show the hardening behavior with decreasing temperature in the ferroelectric phase.[26] Furthermore, if the local ferroelectric region arises, it would induce the additional polarization around itself through an electric dipole-dipole interaction. This effect is considered to enhance the growth of LSBR dramatically. Thus, the additional growth of LSBR observed in the low-temperature region of STO18-32 (Fig. 6) can be concluded to be caused by the occurrence of the local ferroelectric region.

Although the appearance of the local ferroelectric region explains well several anomalies in STO18-32, the temperature dependence of the soft $E_u$ mode still remains unsolved. If the ferroelectric region arises, as mentioned before, the soft $E_u$ mode must undergo freezing. However, the soft $E_u$ mode frequency in STO18-32 does not take zero frequency at any temperature, as shown in Fig. 7(c). Here, it should be noted that the linewidth of the soft $E_u$ mode exhibits clearly a peaklike anomaly with its maximum at 13 K. The maximum of the linewidth takes place before the frequency minimum of the soft $E_u$ mode at 9 K. Such a peaklike anomaly is not observed in STO16 and STO18-23, as shown in Figs. 7(a) and 7(b), indicating the close relation between the hardening behavior and the peaklike anomaly in STO18-32. The temperature dependence of the soft $E_u$ mode frequency is discussed in the following section in connection with the peaklike anomaly of the linewidth of the soft $E_u$ mode spectrum.

### D. Origin of the temperature dependence of the soft $E_u$ mode frequency in STO18-32

In the partially exchanged STO18-$x$, the oxygen isotope $^{18}O$ would be distributed inhomogeneously in the whole volume of the crystal. According to the mass distribution induced by this inhomogeneous distribution of $^{16}O$ and $^{18}O$, the magnitude of the isotope effect is considered to be dis-
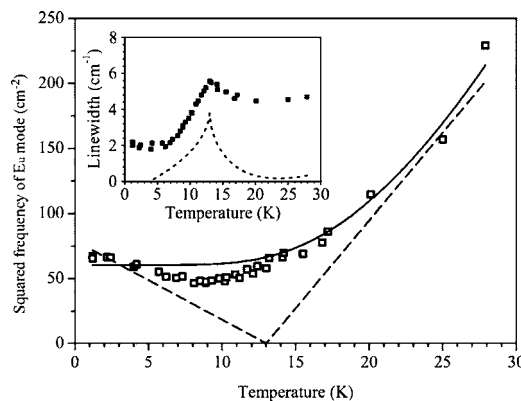


FIG. 8. Square of the soft $E_u$ mode frequency in STO18-32 (open circles). Broken line and solid line are calculated with the Curie-Weiss law and Barrett's formula, respectively. The inset shows the linewidth of the soft $E_u$ mode spectrum in STO18-32 (closed squares) and the difference between the solid line and the broken line (dotted line). See text for details.

tributed locally in the crystal. Therefore, it would be important to take the effect of the inhomogeneous mass distribution into account in the study of the soft-mode dynamics in STO18-$x$. In this section, we discuss the soft $E_u$ mode dynamics in STO18-32 in connection with the inhomogeneous distribution of the oxygen isotope $^{18}O$.

In STO18-32, whose exchange rate is very close to $x_c$, the concentration of $^{18}O$ would exceed locally the critical exchange rate $x_c$. In the region where the local concentration is larger than $x_c$, the quantum fluctuation is considered to be depressed sufficiently to realize the local order. Consequently, in this region, the ferroelectric order is expected to be realized even at finite high temperature. Because the quantum fluctuation becomes no longer effective in this ferroelectric region, the soft $E_u$ mode would obey the Curie-Weiss law of the classical regime in this region. In the other region where the local concentration of $^{18}O$ is less than $x_c$, on the other hand, the local symmetry remains nonferroelectric until 0 K because the quantum fluctuation is still effective to suppress the ferroelectric order. In this nonferroelectric region, the soft $E_u$ mode would follow the temperature dependence given by Barrett's formula of the quantum paraelectric regime as observed in STO18-23. Thus, in the inhomogeneous system of STO18-32, the soft $E_u$ mode is considered to behave in the manner sensitive to the local concentration of the oxygen isotope $^{18}O$.

According to the mechanism mentioned above, we can propose a model which states the Raman spectrum of STO18-32 includes the two types of soft $E_u$ mode spectra: (i) the spectrum of the soft $E_u$ mode in the ferroelectric region, which follows Curie-Weiss law, and (ii) that in the nonferroelectric region, which follows Barrett's formula. On the basis of this model, we have examined the present result for STO18-32. In Fig. 8, the broken line was calculated by the Curie-Weiss law as
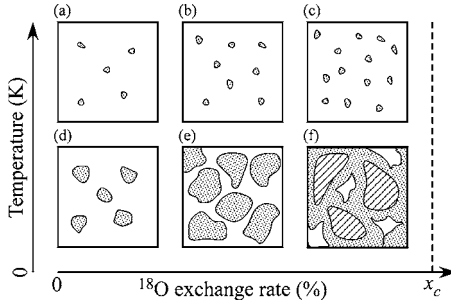
$$\omega_F^2 = A(T - T_c),$$

FIG. 9. Schematic illustration of the development of LSBR. White background, dotted regions, and hatched regions denote the paraelectric region, nonferroelectric LSBR, and local ferroelectric regions, respectively.

where $T_c$ is assumed to be 13 K, the temperature at which the observed linewidth has the maximum value. The calculation by the least-squares method is performed with all data points except those around 13 K. The best-fit lines were given with $A=13.5$ for $T>T_c$ and with $A=6.1$ for $T<T_c$.

The solid line was calculated by the square of Barrett's formula as

$$\omega_{NF}^2 = C\left\{\frac{T_1}{2}\coth\left(\frac{T_1}{2T}\right) - T_0\right\}.$$

The calculation using the least-squares method with all data points converged with $C=5.5$, $T_1=78.0$ K, and $T_0=37.0$ K, which are in good agreement with the values reported previously.[8] In the present model, since the observed spectrum is given by the superposition of the two kinds of $E_u$ mode spectra, the apparent linewidth of the soft $E_u$ mode spectrum is related to the interval between the peak positions of the two spectra. Therefore, if the present model is valid, the peaklike anomaly would be explained by the difference between the frequencies of two kinds of $E_u$ modes. The difference between each frequency, $\omega_{NF}-\omega_F$, is presented by a dotted line in the inset of Fig. 8. As shown in the inset, the dotted line reproduces qualitatively the peaklike anomaly of the linewidth. This result indicates the validity of the present model.

Next, we discuss the temperature dependence of the soft $E_u$ mode frequency on the basis of the present model. In STO18-32, two kinds of LSBR, namely the ferroelectric region and the nonferroelectric region, are considered to exist in the crystal, as mentioned above. Therefore, the Raman spectrum is observed as a superposition of the two kinds of $E_u$ mode spectra from these regions. Since the intensity of the soft $E_u$ mode spectrum is proportional to the size of LSBR in the quantum paraelectric STO18-$x$ $(x<x_c)$, the observed spectral shape is determined by the ratio of each region in the scattering volume. In the low-temperature region below 13 K, the ferroelectric region would develop markedly, because the polarization induced by the freezing of the Slater-type polar mode is considered to induce the additional polarizations around itself through the electric dipole-dipole interaction. Consequently, the soft $E_u$ mode spectrum which obeys the Curie-Weiss law (broken line in Fig. 8) starts to be

observed dominantly in the low-temperature region. In the high-temperature region above 13 K, on the other hand, the soft $E_u$ mode spectrum which obeys Barrett's formula (solid line in Fig. 8) is considered to be dominant, because the ferroelectric region would not grow so much yet. Thus, the temperature dependence of the soft $E_u$ mode frequency in STO18-32 denoted by open squares in Fig. 8 can be explained as follows: the hardening behavior in the low-temperature region is caused by the soft $E_u$ mode in the ferroelectric region, and the nonfreezing behavior is due to that of the soft $E_u$ mode in the nonferroelectric region. Finally, we can conclude that the local ferroelectric region in STO18-32 is induced by the local softening of the Slater-type polar mode.

### E. Isotope-exchange effect on the local symmetry breaking

From the present results, we can illustrate the process of the isotopic induction of ferroelectricity as shown in Fig. 9. In the figure, the centrosymmetric region, nonferroelectric LSBR, and local ferroelectric region are denoted by a white background, a dotted region, and a hatched region, respectively. First, as presented in Figs. 9(a), 9(b), and 9(c), the embryo of LSBR is considered to be formed around the defect such as an oxygen vacancy, a dislocation, and so on. The amount of the embryo is considered to increase with the exchange rate as illustrated in the figures, because the process of the redox would increase the defects in the crystal. In the low-temperature region of nonexchanged STO16, LSBR does not grow so much due to relatively strong quantum fluctuation [Fig. 9(d)]. By the exchange of $^{16}O$ for $^{18}O$, the quantum fluctuation is decreased and LSBR starts to grow markedly in the low-temperature region [Fig. 9(e)]. Furthermore, in the exchange rate just below $x_c$, the quantum fluctuation becomes depressed enough locally. Consequently, the local ferroelectric region is induced precursorily before the onset of the ferroelectric order as presented in Fig. 9(f). With a further increase of the exchange rate, the long-range order of polarization is expected to take place. In contrast to the drastic change in the low-temperature region, the present results indicate that the local symmetry breaking is insensitive to the isotope exchange in the high-temperature region. This fact confirms that the drastic isotope effect on the local symmetry breaking is caused by the depression of quantum fluctuation by the isotope exchange because quantum fluctuation is considered to become dominant, especially in the low-temperature region.

### V. CONCLUSION

In the present study, we investigate the isotope effect on the soft-mode dynamics and the local symmetry breaking in STO18-$x$, and obtain the following conclusions: (i) the lattice vibration of the Slater-type polar mode becomes destabilized with increasing the exchange rate of $^{18}O$, (ii) the quantum fluctuation is apparently depressed by the isotope exchange,

and (iii) the isotope exchange renders the system inhomogeneous by the spatially nonuniform mass distribution of the oxygen atoms. By these factors, the local ferroelectric region is induced precursorily by the inhomogeneous softening of the Slater-type polar mode before the onset of the ferroelectric phase transition.

*Electronic address: mmb@es.hokudai.ac,jp

[1] K. A. Müller and H. Burkard, Phys. Rev. B **19**, 3593 (1979).

[2] K. A. Müller, W. Berlinger, and E. Tossatti, Z. Phys. B: Condens. Matter **84**, 277 (1991).

[3] N. Sai and D. Vanderbilt, Phys. Rev. B **62**, 13942 (2000).

[4] P. A. Fleury and J. M. Worlock, Phys. Rev. **174**, 613 (1968).

[5] H. Uwe and T. Sakudo, Phys. Rev. B **13**, 271 (1976).

[6] M. Itoh, R. Wang, Y. Inaguma, T. Yamaguchi, Y.-J. Shan, and T. Nakamura, Phys. Rev. Lett. **82**, 3540 (1999).

[7] M. Itoh and R. Wang, Appl. Phys. Lett. **76**, 221 (2000).

[8] R. Wang and M. Itoh, Phys. Rev. B **64**, 174104 (2001).

[9] K. Yamanaka, R. Wang, and M. Itoh, J. Phys. Soc. Jpn. **70**, 3213 (2001).

[10] E. L. Venturini, G. A. Samara, M. Itoh, and R. Wang, Phys. Rev. B **69**, 184105 (2004).

[11] L. Zhang, W. Kleemann, J. Dec, R. Wang, and M. Itoh, Eur. Phys. J. B **28**, 163 (2002).

[12] J. Hemberger, M. Nicklas, R. Viana, P. Lunkenheimer, A. Loidl, and R. Böhmer, J. Phys.: Condens. Matter **8**, 4673 (1996).

[13] A. Bussmann-Holder, H. Büttner, and A. R. Bishop, J. Phys.: Condens. Matter **12**, L115 (2000).

[14] Y. Yamada, N. Todoroki, and S. Miyashita, Phys. Rev. B **69**, 024103 (2004).

[15] T. Yagi, M. Kasahara, Y. Tsujimi, H. Hasebe, M. Yamaguchi, R. Wang, and M. Itoh, MRS Symposia Proceedings No. 718 (Materials Research Society, 2002), p. 183.

[16] T. Yagi, M. Kasahara, Y. Tsujimi, H. Hasebe, M. Yamaguchi, R. Wang, and M. Itoh, Physica B **316-317**, 596 (2002).

[17] M. Takesada, M. Itoh, and T. Yagi (unpublished).

[18] H. Taniguchi, M. Takesada, M. Itoh, and T. Yagi, J. Phys. Soc. Jpn. **73**, 3262 (2004).

[19] H. Taniguchi, M. Takesada, M. Itoh, and T. Yagi, J. Korean Phys. Soc. **46**, 195 (2005).

[20] G. Shirane and Y. Yamada, Phys. Rev. **177**, 858 (1969).

[21] T. Sekine, K. Uchinokura, and E. Matsuura, Solid State Commun. **18**, 569 (1976).

[22] H. Uwe, H. Yamaguchi, and T. Sakudo, Ferroelectrics **96**, 123 (1989).

[23] K. Inoue and N. Asai, J. Phys. (Paris), Colloq. **42**, C6-430 (1981).

[24] H. Uwe, Jpn. J. Appl. Phys., Suppl. **24–2**, 513 (1985).

[25] M. Kasahara, R. Wang, M. Ioth, and T. Yagi, J. Phys. Soc. Jpn. **71**, 1254 (2002).

[26] W. Cochran, Phys. Rev. Lett. **3**, 412 (1959).